2018 26th Mediterranean Conference on Control and Automation (MED)
Zadar, Croatia, June 19-22, 2018

Design of a weighted multi-controller for lateral guidance of autonomous vehicles using steering control

Nolwenn Monot, Xavier Moreau, André Benine-Neto, Audrey Rizzo, and François Aioun

Abstract— **This study proposes a new approach to control the vehicle lateral position at all speeds. The influence of the longitudinal speed on the vehicle lateral dynamics is taken into account to the design of the controller. The strategy developed uses several PID, weighted in function of the longitudinal speed enabling the vehicle to drive either at high or low speed. A methodology based on stability margin is proposed in order to design the intervals of longitudinal speed used for the multi-controller. The multi-controller is compared to a single PID and a simulation shows that for an overtaking with speed variation, when the weighted multi-controller manage to track the desired trajectory, the PID alone cannot follow it.**

I. INTRODUCTION

The steering of the automotive vehicles has been subject to many researches and evolutions. Among them, the steering assist system helps the driver to steer by reducing the steering effort needed to the rotation of the wheels. Several technologies of steering assist system have been used, such as hydraulic systems, electro-hydraulic system, electric system or steer-by-wire system. In the last category, the mechanical linkage between the wheels and the steering wheel is completely replaced by electrical systems.

Now, in the context of the autonomous and intelligent vehicle, the objective of many researches is to completely control the steering column, under every situation and without human interaction. The researches differ in terms of considered environments, control strategies and robustness.

Many papers treat the lateral control of the vehicle in highway scenario ([1] and [2]) because it is the easiest road environment: traffic in a single direction, large radius of curvature and few use cases. Urban environments have started to be studied, particularly in the case of the roundabouts ([3] and [4]).

The controllers used for the regulation of the lateral position of the vehicle are various. The subject has been covered with the classic proportional integrator ([4]), adaptive proportional derivative ([5]) or gain scheduled proportional ([2]). Other classic regulation methods have been explored such as: model predictive control in [6], H_∞ control in [7] and [1], sliding mode control in [8] and linear quadratic command in [9]. Even approaches applied in artificial intelligence and machine learning have been used for this topic as in [3] and [10] that use fuzzy-logic and [11] that uses neural network.

Some papers examine the robustness of their controllers with respect to uncertain parameters. In [5], the parameters of the PD controller vary as a function of the longitudinal speed in order to minimize the output error. In [7], the system is robust to the road adhesion and the speed but the robustness is evaluated after the calculation of the controller. Similarly as in [6] the uncertain parameters do not vary in the simulations.

Other researches have already applied multi-regulation for steering control. In [12] a state feedback multi-controller is presented. Each controller is computed with the minimization of quadratic Lyapunov functions using LMI (Linear Matrix Inequality) and a switch selects the controller based on the estimation of the wheel slip angle. Switches can be avoided by using Takagi-Sugeno approach for the design of the multi-controller, as in [13]. The subsystems are function of the cornering stiffness and their controllers are also computed using LMI. However, none of these researches treated the variation of longitudinal speed. Although several constraints can be added to these kind of optimisation problems, as an attempt to refine the design of the controller, they tend to be conservative, often resulting in numerical problems. Even when a solution is provided, the complexity of the problem prevents the designer from actually understanding the effect of each parameter of the controller.

Among these papers, few study the lateral dynamics of the vehicle before developing their strategies. In fact, the longitudinal speed has a significant influence on this dynamics and should be taken into consideration for the design of the controller. The objective of this study is to design a lateral controller for an autonomous vehicle, robust to the significant longitudinal speed variations (from 1 to 130 km/h). The two main contributions are: firstly, it provides an analysis on the influence of the vehicle longitudinal velocity on its lateral dynamics, so that it can be taken into account to the design phase of the controller, instead of an a posteriori verification for robustness. Secondly the proposed controller has a simple structure based on a multi-PID weighted as a function of the longitudinal velocity, such that not only the effect of each parameter is fully understood but also it can be easily implemented in the industrial context.

The paper is organized as follows. Section II describes the vehicle lateral dynamics and section III analyzes this dynamics in the frequency domain. In section IV, the design of the controllers are described and section V makes the

N. Monot is with IMS Laboratory, Univ. Bordeaux, Bordeaux INP, CNRS, UMR 5218, 33405 Talence, France and also with Groupe PSA, 78943 Velizy-Villacoublay, France (e-mail: name.surname@mpsa.com).

X. Moreau and A. Benine-Neto are with IMS Laboratory, Univ. Bordeaux, Bordeaux INP, CNRS, UMR 5218, 33405 Talence, France (e-mail: name.surname@ims-bordeaux.fr).

A. Rizzo and F. Aioun are with Groupe PSA, 78943 Vélizy-Villacoublay, France (e-mail: name.surname@mpsa.com).

This work took place in the framework of the OpenLab 'Electronics and System for Automotive' combining IMS Laboratory and the Groupe PSA company.

comparison with an overtaking maneuver. Section VI wraps up the paper with conclusions and perspectives.

II. Lateral dynamic equations

The equation describing the yaw dynamic is given by:

$$\dot{\Psi}(t) = \frac{1}{I_z}\int_0^t C_{\Sigma z}(\tau)d\tau + \dot{\Psi}(0), \tag{1}$$

where I_z is the moment of inertia and $C_{\Sigma z}(t)$ is the sum of external torques around the vehicle vertical axis such that:

$$\begin{aligned} C_{\Sigma z}(t) =& L_f\left(F_{y11}(t) + F_{y12}(t)\right)\cos(B_v(t)) \\ &- L_r\left(F_{y21}(t) + F_{y22}(t)\right) \\ &+ l_f\left(F_{x12}(t) - F_{x11}(t)\right)\sin(B_v(t)) \\ &+ l_r\left(F_{x22}(t) - F_{x21}(t)\right), \end{aligned} \tag{2}$$

with L_f and L_r the front and rear wheelbases. l_f and l_r are the front and rear half track width of the vehicle. $B_v(t)$ is the steering angle. The forces $F_x(t)$ and $F_y(t)$ are respectively the longitudinal and lateral forces applied on the tyres and the subscripts refer to the tyres as illustrated in Fig 1.

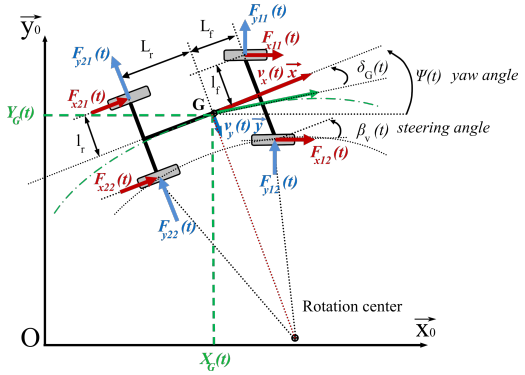

Fig. 1. Forces scheme

Considering a vehicle traveling at longitudinal speed, $V_x(t)$, the lateral velocity dynamics is described by:

$$V_y(t) = \frac{1}{M_t}\int_0^t F_{\Sigma y}(\tau)d\tau - \int_0^t V_x(t)\dot{\Psi}(\tau)d\tau + V_y(0), \tag{3}$$

where M_t is the mass of the vehicle and $F_{\Sigma y}(t)$ the sum of the exterior forces at the center of gravity around the vehicle lateral axis, as follows:

$$\begin{aligned} F_{\Sigma y}(t) =& \left(F_{y11}(t) + F_{y12}(t)\right)\cos(\beta_v(t)) \\ &+ F_{y21}(t) + F_{y22}(t) + f_{0y}(t), \end{aligned} \tag{4}$$

where $f_{0y}(t)$ represents the equivalent of a disturbance force (such as a wind gust) applied at the vehicle center of gravity.

Tyre forces are described according to Pacejka's model [14]. The equation between the lateral force $F_{yij}(t)$ and the associated tyre slip angle $\Delta_{ij}(t)$ is given by:

$$\begin{aligned} F_{yij}(t) = \mu(t)D_{yij}\sin\Bigg[C_{yij}\text{atan}\Big(B_{yij}\Big[(1-E_{yij})\Delta_{ij}(t) \\ + \frac{E_{yij}}{B_{yij}}\text{atan}(B_{yij}\Delta_{ij}(t))\Big]\Big)\Bigg], \end{aligned} \tag{5}$$

where the macro-parameters D_{yij}, C_{yij}, B_{yij} and E_{yij} depend on the tyre's micro-parameters, the normal force $F_z(t)$ and the road adhesion $\mu(t)$.

The tyres slip angles used in (5) are obtained with:

$$\begin{aligned} \Delta_{11}(t) &= B_v(t) - \text{atan}\left(\frac{V_y(t) + \dot{\Psi}(t)L_f}{V_x(t) - l_f\dot{\Psi}(t)}\right) \\ \Delta_{12}(t) &= B_v(t) - \text{atan}\left(\frac{V_y(t) + \dot{\Psi}(t)L_f}{V_x(t) + l_f\dot{\Psi}(t)}\right) \\ \Delta_{21}(t) &= -\text{atan}\left(\frac{V_y(t) - \dot{\Psi}(t)L_r}{V_x(t) - l_r\dot{\Psi}(t)}\right) \\ \Delta_{22}(t) &= -\text{atan}\left(\frac{V_y(t) - \dot{\Psi}(t)L_r}{V_x(t) + l_r\dot{\Psi}(t)}\right). \end{aligned} \tag{6}$$

The steering angle $B_v(t)$ is proportional to the steering-wheel angle $\Theta_v(t)$ such that:

$$\Theta_v(t) = \lambda B_v(t), \tag{7}$$

with λ the steering column gear ratio.

The vehicle trajectory is defined by the coordinates $X_G(t)$ and $Y_G(t)$ of the gravity center in the absolute frame of reference $R_0 = (O, \overrightarrow{x_0}, \overrightarrow{y_0})$. $R = (G, \overrightarrow{x}, \overrightarrow{y})$ the frame of reference of the vehicle. These coordinates are calculated with the integration of the gravity center's velocity:

$$\begin{aligned} \overrightarrow{V}_{G/R_0} = V_{x0}\overrightarrow{x} + V_y(t)\overrightarrow{y} &= \left[\frac{d\overrightarrow{OG}}{dt}\right]_{R_0} \\ &= \left[\frac{d}{dt}\left(X_G(t)\overrightarrow{x_0} + Y_G(t)\overrightarrow{y_0}\right)\right]_{R_0} \\ &= \dot{x}_G(t)\overrightarrow{x_0} + \dot{y}_G(t)\overrightarrow{y_0}. \end{aligned} \tag{8}$$

The equations changing the frame of reference from R_0 to R are:

$$\begin{cases} \overrightarrow{x} = \cos\left(\Psi(t)\right)\overrightarrow{x_0} + \sin\left(\Psi(t)\right)\overrightarrow{y_0} \\ \overrightarrow{y} = -\sin\left(\Psi(t)\right)\overrightarrow{x_0} + \cos\left(\Psi(t)\right)\overrightarrow{y_0}. \end{cases} \tag{9}$$

So the derivative of the coordinates of the gravity center's in the absolute frame of reference are:

$$\begin{cases} \dot{x}_G(t) = V_x(t)\cos\left(\Psi(t)\right) - V_y(t)\sin\left(\Psi(t)\right) \\ \dot{y}_G(t) = V_x(t)\sin\left(\Psi(t)\right) + V_y(t)\cos\left(\Psi(t)\right). \end{cases} \tag{10}$$

Finally, the coordinates of the gravity center are obtained

with the integration of (10):

$$\begin{cases} x_G(t) = \int_0^t \left(V_x(t)\cos\left(\Psi(\tau)\right) - V_y(\tau)\sin\left(\Psi(\tau)\right)\right) d\tau \\ \qquad + X_G(0) \\ y_G(t) = \int_0^t \left(V_x(t)\sin\left(\Psi(\tau)\right) + V_y(\tau)\cos\left(\Psi(\tau)\right)\right) d\tau \\ \qquad + Y_G(0). \end{cases} \tag{11}$$

TABLE I
PARAMETERS OF THE DYNAMIC SYSTEM

V_{x0}	Longitudinal speed	Between 1 km/h and 130 km/h
μ	Road adhesion	1
M_t	Total mass of the vehicle	1759 kg
$M_{f/r}$	Front / rear mass	1319 kg / 439 kg
I_z	Moment of inertia	2638 $\mathrm{kg.m^2}$
$L_{f/r}$	Front / rear wheelbase	0.71 m / 2.13 m
$c_{yf/r}$	Front / rear lateral cornering stiffness	94446 $\mathrm{N.rad^{-1}}$ / 48699 $\mathrm{N.rad^{-1}}$
λ	Steering column gear rate	16

III. ANALYSIS OF THE LATERAL DYNAMICS

A. Linearization

In order to analyze the lateral dynamics of the vehicle and design the controllers in the frequency domain, the equations describing these dynamics must me linearized. For that, the longitudinal speed is considered constant such that $V_x(t) = V_{x0}$.

Five equations contain non-linear functions: the expressions of $C_{\Sigma z}(t)$ in (2), $F_{\Sigma y}(t)$ in (4), $F_{yij}(t)$ with Pacejka in (5), $\Delta_{ij}(t)$ in (6) and the trajectory in (10) and (11).

In the case of overtaking maneuvers with constant longitudinal speed, simulations (as in [15]) show that the tyres are in a linear operating area for all the speeds between 1 km/h and 130 km/h. Thus, (5) can be rewritten:

$$F_y(t) = c_y \Delta_t(t), \tag{12}$$

where c_y is the cornering stiffness defined as $c_y = \mu B_y C_y D_y$.

Considering $\left|\frac{l}{2}\dot{\Psi}(t)\right| << V_{x0}$, and under small angle assumption (which can also be verified through simulation of a lane-change manoeuvre, as in [15]), the expressions of tyre sideslip angles (6) can be written as:

$$\begin{aligned} \Delta_{11}(t) = \Delta_{12}(t) = \Delta_f(t) &\approx B_v(t) - \frac{V_y(t) + L_f\dot{\Psi}(t)}{V_{x0}} \\ \Delta_{21}(t) = \Delta_{22}(t) = \Delta_r(t) &\approx -\frac{V_y(y) - L_r\dot{\Psi}(t)}{V_{x0}}, \end{aligned} \tag{13}$$

which yields to a single track (bicycle) model.

The small angle assumption also enables the linearization of equations (2), (4), (10) and (11). It gives respectively:

$$C_{\Sigma z}(t) = L_f\left(F_{y11}(t) + F_{y12}(t)\right) - L_r\left(F_{y21}(t) + F_{y22}(t)\right), \tag{14}$$

$$F_{\Sigma y}(t) = F_{y11}(t) + F_{y12}(t) + F_{y21}(t) + F_{y22}(t) + f_{0y}(t), \tag{15}$$

$$\dot{y}_G(t) = V_{x0}\Psi(t) + V_y(t), \tag{16}$$

and

$$y_G(t) = \int_0^t \left(V_{x0}\Psi(t) + V_y(\tau)\right) d\tau + Y_G(0). \tag{17}$$

B. Linear Model in Frequency domain

With the linearized equations, the lateral dynamics of the vehicle can be expressed in a linear state-space representation. The state vector is $\underline{x}(t) = \begin{pmatrix} \psi(t) \\ \dot{\psi}(t) \\ v_y(t) \\ y_G(t) \end{pmatrix}$, and the input control $u(t) = \theta_v(t)$. The objective is the regulation of the lateral position through the steering-wheel. Hence, the output is $y(t) = y_G(t)$ and the following state-space representation is defined:

$$\begin{cases} \dot{\underline{x}}(t) = A\underline{x}(t) + Bu(t) \\ y(t) = C\underline{x}(t), \end{cases} \tag{18}$$

with

$$A = \begin{bmatrix} 0 & 1 & 0 & 0 \\ 0 & -\frac{2(L_f^2 c_{yf} + L_r^2 c_{yr})}{I_z V_{x0}} & -\frac{2PDE}{I_z V_{x0}} & 0 \\ 0 & -\frac{2PDE}{M_t V_{x0}} - V_{x0} & -\frac{2(c_{yf} + c_{yr})}{M_t V_{x0}} & 0 \\ V_{x0} & 0 & 1 & 0 \end{bmatrix},$$

$$B = \begin{bmatrix} 0 \\ \frac{2c_{yf}L_f}{\lambda I_z} \\ \frac{2c_{yf}}{\lambda M_t} \\ 0 \end{bmatrix} \text{ and } C = \begin{bmatrix} 0 & 0 & 0 & 1 \end{bmatrix}, \tag{19}$$

with $PDE = L_f c_{yf} - L_r c_{yr}$.

The transfer function used for the controllers design is $G(s) = \frac{Y_G(s)}{\Theta_v(s)}$. It can be obtained with the relations (19) using the equation:

$$G(s) = \frac{Y_G(s)}{\Theta_v(s)} = C[sI - A]^{-1}B. \tag{20}$$

The transfer function $G(s)$ is plotted on a bode diagram on Fig. 2 for different values of V_{x0}. These frequency responses of the linearized models show that the longitudinal speed has an important influence on the lateral dynamics, with about 78 dB of gain variations at low frequency, and over 138°

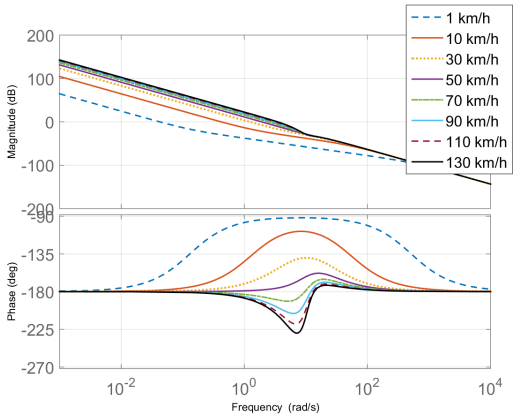

Fig. 2. Bode diagram of $G(s)$

of phase variation at 7 rad/s. The effect of the longitudinal speed on the lateral dynamics is not only noticeable by the different values of the frequency responses, it also affects its behavior, since $G(s)$ is a natural phase-lead system for low speeds and it becomes a phase-lag system for higher speeds. Moreover it is important to point out that, for a given frequency (for instance, 7 rad/s) and similar speed intervals, the phase variation is greater at lower speeds (about $92.5°$ for a speed range from 1 to 65 km/h) than for higher speeds (about $40°$ for the speed range from 65 to 130 km/h).

The analytical equation of $G(s)$ is:

$$G(s) = \frac{K_0}{s^2}\frac{1+2\zeta_1(s/\omega_1)+(s/\omega_1)^2}{1+2\zeta_0(s/\omega_0)+(s/\omega_0)^2}, \tag{21}$$

where the coefficients K_0, ζ_0, ζ_1, ω_0 and ω_1 can be expressed according to the vehicle parameters, the road adhesion and the longitudinal speed such that:

$$\begin{aligned}
K_0 &= \frac{2c_{yf}c_{yr}V_{x0}^2L}{\lambda(2c_{yf}c_{yr}L^2 - M_tV_{x0}^2PDE)},\\
\zeta_0 &= \frac{M_t(L_f^2c_{yf}+L_r^2c_{yr})+I_z(c_{yf}+c_{yr})}{\sqrt{2I_zM_t(2c_{yf}c_{yr}L^2-M_tV_{x0}^2PDE)}},\\
\omega_0 &= \sqrt{2}\sqrt{\frac{2c_{yf}c_{yr}L^2-M_tV_{x0}^2PDE}{I_zM_tV_{x0}^2}},\\
\zeta_1 &= \frac{L_f}{V_{x0}}\sqrt{\frac{c_{yr}L}{2I_z}},\\
\omega_1 &= \sqrt{2\frac{c_{yr}L}{I_z}},
\end{aligned} \tag{22}$$

with $L = L_f + L_r$. Except for ω_1, all the parameters of the transfer function $G(s)$ depend on V_{x0}. The variations of these parameters in function of the longitudinal speed are plotted on Fig. 3 and 4.

It can be observed on Fig. 4 that the transitional frequency ω_0 becomes smaller than ω_1 for speeds higher than 65 km/h, explaining the change between the phase lead and the phase lag systems observed on Fig. 2. The damping factor ζ_0 can be seen on Fig. 4 (b), it shows that the system is under damped when $V_{x0} > 30$ km/h and damped when $V_{x0} < 30$ km/h.

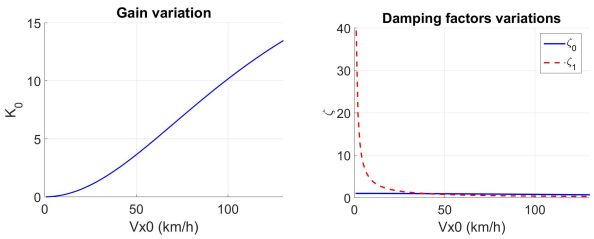

(a) (b)

Fig. 3. Variation of the gain K_0 (a) and ζ (b) as a function of the longitudinal speed V_{x0}

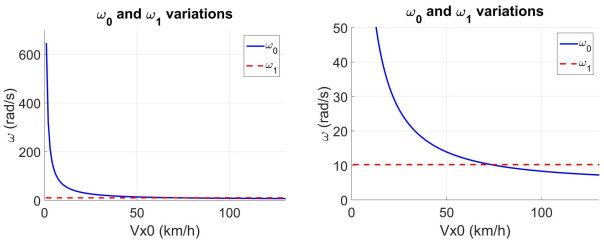

(a) (b)

Fig. 4. Variation of the pulsations ω_0 and ω_1 (a) as a function of the longitudinal speed V_{x0} and a zoom (b)

IV. Design of the Controller

In order to enhance the lateral regulation performance, the significant phase variation of $G(s)$ with respect to the longitudinal speed must be taken into account in the design of the controller. In this section two controllers are designed: a regular PID, for comparison purposes, computed with the transfer function of the model linearized around the speed $V_{xPID} = 90$ km/h and a multi PID that should be able to regulate the lateral position of the vehicle at all speed.

A. Specification

The parameters needed for the design of PIDs are: the crossover open-loop frequency ω_u and the phase margin M_Φ. ω_u is chosen in order to respect a human behavior dynamic of the steering-wheel: $\omega_u = 1$ rad/s and M_Φ is chosen as the empiric value $M_\Phi = 45°$ known to guarantee a good stability.

B. Design of a classic PID

This PID is computed for the system linearized around $V_{xPID} = 90$ km/h. This speed was chosen because of the highway scenario.

$$C(s) = C_0\frac{1+(s/\omega_i)}{(s/\omega_i)}\frac{1+s/\omega_l}{1+s/\omega_h}, \tag{23}$$

where C_0 is a proportional gain, ω_i such that $\omega_i = \omega_u/10$ is the transitional frequency, ω_l and ω_h are the transitional frequencies of the lead or lag compensator.

Knowing that the open-loop transfer function is written:

$$\beta(j\omega) = C(j\omega)G(j\omega), \tag{24}$$

the frequencies ω_l and ω_h are calculated in the respect of the desired phase margin:

$$M_\Phi = \arg\Big(\beta(j\omega_u)\Big) + \pi, \tag{25}$$

with

$$\arg\Big(\beta(j\omega_u)\Big) = \arg\Big(C(j\omega_u)G(j\omega_u)\Big) \\ = \arg\Big(C(j\omega_u)\Big) + \arg\Big(G(j\omega_u)\Big). \quad (26)$$

The lead/lag cell of the PID controller brings a phase ϕ_m at the frequency $\omega_m = \sqrt{\omega_l \omega_h}$, expressed as:

$$\phi_m = M_\Phi - \frac{\pi}{2} - \arg\Big(G(j\omega_u)\Big) - \text{atan}\Big(\frac{\omega_u}{\omega_i}\Big), \quad (27)$$

with $\omega_u = \omega_m$. Knowing that

$$\alpha = \frac{1+\sin\phi_m}{1-\sin\phi_m}, \quad (28)$$

ω_l and ω_h can be written:

$$\omega_l = \omega_u\sqrt{\alpha}, \quad \omega_h = \omega_u/\sqrt{\alpha}. \quad (29)$$

The gain C_0 is obtained with the relation:

$$\Big|\beta(j\omega_u)\Big| = \Big|C(j\omega_u)G(j\omega_u)\Big| = 1. \quad (30)$$

C. Design of a weighted multi-PID

Based on the phase variations of the linearized system about different longitudinal speeds (21), as shown in Fig. 2, the classical PID controller is not even able to ensure the stability for all considered speeds, as it can be seen on Fig. 7 (a) and 8 (a) (do not satisfy Nyquist criteria of stability for V_{x0} = 1 or V_{x0} = 10 km/h). In fact a single PID cannot overcome the important phase variation of $G(s)$ for different speeds. Therefore, the main idea of this paper is to design a multi-PID robust to the longitudinal speed change.

It has been shown in [16] that switched controllers could bring instability depending on the frequency of the switches. In this case, in order to keep continuity between the different PID, weights are used on each PID, enabling their gradual (de-)activation. The objective being the robustness of the controller to the variation of the longitudinal speed, the proposed weights are functions of $V_x(t)$.

The difficulty of this method is to find the right number of PID, for which speed they should be designed and how to define the weights of each PID. Since significant phase variation of $G(s)$ for different longitudinal speeds prevents the system from being stabilized with a single PID, such variations are taken into account in the design of the proposed multi-controller. Fig. 5 (a) shows $\arg G(j\omega_u)$ as a function of the vehicle longitudinal speed. Due to the noticeable nonlinear characteristic, it is reasonable to choose the operating points for the design of each PID based on phase variation of $G(j\omega_u)$, instead of regular speed-based intervals, as frequently applied in gain scheduling solution [17]. It is important to remark that the proposed choice of speed intervals is able to reduce the effect of the phase variation more equally throughout the whole range of longitudinal speed.

Fig. 5 (b) shows the constant phase intervals chosen for the vehicle lateral control. A variation of $Var_\phi = 15°$ was arbitrarily chosen in order to provide a reasonable trade-off between the closed loop performance and the complexity

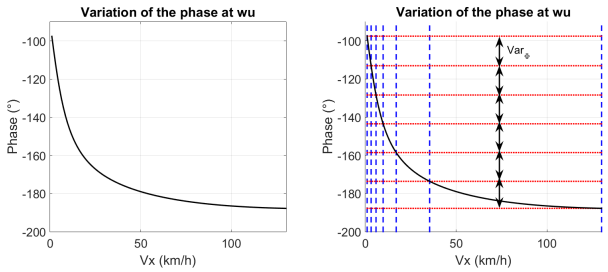

(a) (b)

Fig. 5. Variation of $G(j\omega_u)$ phase in function of the speed (a) and the cutting used for the choice of the speeds operating points (b)

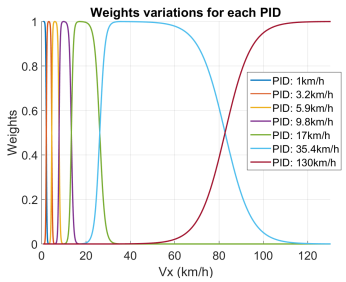

Fig. 6. Variations of each PID weights in function of the speed

of the multi-controller. This choice lead to 6 intervals, so 7 PID. The speeds for which each PID is designed are $V_{xint} = \{1; 3.2; 5.9; 9.8; 17; 35.4; 130\}$ km/h. Each PID has the form (23) with their parameters computed with (26)-(30).

Unlike in fuzzy logic, the weights of the PID designed in this paper do not vary linearly through the decision variable in each intervals. Instead, in order to maintain the continuity at the speeds in V_{xint} sigmoid functions are used. A sigmoid $f_\gamma(x)$, with $x \in \mathbb{R}$, $\gamma \in \mathbb{R}$, is written:

$$f_\gamma(x) = \frac{1}{1+e^{-\gamma x}}. \quad (31)$$

For the ith PID, his weight ξ_i is calculated so that:

$$\xi_i(V_x) = 1 - f_{\gamma_i}(V_x) + f_{\gamma_{i-1}}(V_x), \quad (32)$$

with $1 - f_{\gamma_i}(V_x)$ the sigmoid on the interval $[V_{xint}(i); V_{xint}(i+1)]$ and $f_{\lambda_{i-1}}(V_x)$ the sigmoid on the interval $[V_{xint}(i-1); V_{xint}]$. Finally, the weighted PID can be written as:

$$PID(s) = \sum_{i=1}^{7} \xi_i(V_x) PID_i(s), \quad (33)$$

and this leads to the weights plotted on Fig. 6.

D. Comparison in the frequency domain

The Bode plots on the Fig. 7 show that there is a significant variation of the open-loop crossover frequency with the classic PID calculated for V_x = 90 km/h. When at high speeds the controller manages to keep an ω_u around 1rad/s, it decreases with the diminution of the speed. At V_x = 1 km/h the open-loop crossover frequency is 100 times smaller than the desired one. For the weighted multi-PID, ω_u varies

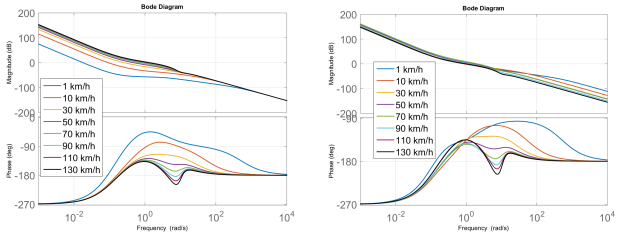

(a) (b)

Fig. 7. Bode diagram of the open-loop with different operating points with the classic PID (a) and the weighted multi-PID (b)

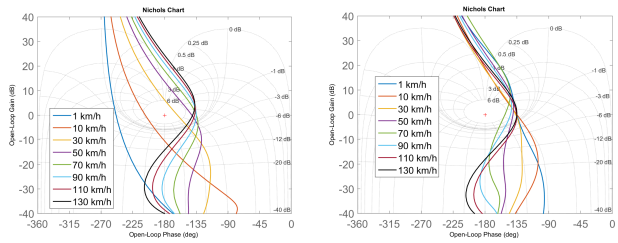

(a) (b)

Fig. 8. Nichols charts of the open-loop with different operating points with the classic PID (a) and the weighted multi-PID (b)

between 0.85rad/s and 2.2rad/s, which is much closer to the specifications.

The stability can be analyzed with the Nichols charts on Fig 8. It appears that the closed system with the designed classic PID is unstable at low speeds. Indeed, with the integration, the PID brings a phase of $-90°$ at low frequencies. This leads to a negative phase margin and so, the instability of the closed-loops with a small ω_u, i.e at small speed. In contrast, the phase margin remains positive at all speeds for the weighted multi-PID with a phase margin superior to $32°$.

V. Simulation Results

In this section, the two designed controllers are compared with a simulation of an overtaking with a variation of the longitudinal speed.

The bloc scheme of the simulation is presented in Fig. 9. The input $Y_{Gref}(t)$ is a 5th order polynomial function, designed in [18], such that:

$$Y_{Gref}(t) = -D_y\left(-10\left(\frac{t}{T}\right)^3 + 15\left(\frac{t}{T}\right)^4 - 6\left(\frac{t}{T}\right)^5\right), \quad (34)$$

with D_y the desired position at the end of the overtaking and T the time in which the vehicle will reach D_y. $\epsilon(t)$ is the output error. For this simulation, the 4-wheels non-linear model of the vehicle lateral dynamics is used. The lateral dynamics follow the description in Section II. Even if the vehicle can be subject to variations of parameters including the mass, the road adhesion or the longitudinal speed. In this subject, only the speed V_x will vary.

For the weighted multi-PID, the bloc scheme of the controller can be seen in Fig. 10.

During the overtaking maneuver, the longitudinal speed $V_x(t)$ varies linearly from 5 km/h to 50 km/h, as shown on

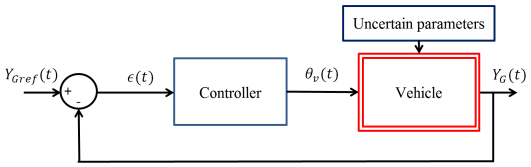

Fig. 9. Bloc scheme of the simulation

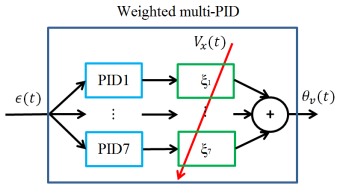

Fig. 10. Bloc scheme of the weighted multi-PID

Fig. 12 (a). The simulation at low speed enables to analyze the influence of the weight changes on the multi-PID, and the response of the classic PID in a different operating point for which it has been designed.

The output and the output error for both controllers are presented on Fig 11 (a) and Fig 11 (b). The multi-PID manages a better regulation of the lateral position with a most extreme error of 45 cm at $t = 8$ s, whereas the most extreme error for the single PID reaches 1.6m at $t = 7$ s. Indeed, observing the Bode diagrams of the open-loop with the classic PID (Fig. 7 (a)), it is possible to notice that the open-loop crossover frequency is lower at low speeds. Because of that, the classic PID is slow to follow the input in the beginning of the overtaking. With the weighted multi-PID, the output error is more than three time smaller than with the classic PID.

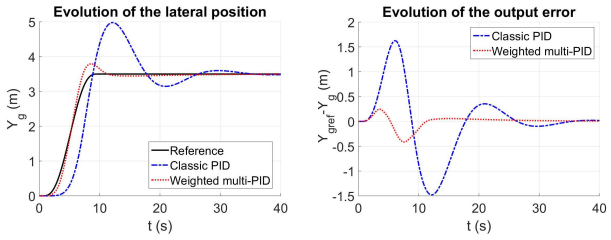

(a) (b)

Fig. 11. Evolution of the lateral position (a) and the output error (b) in function of the time

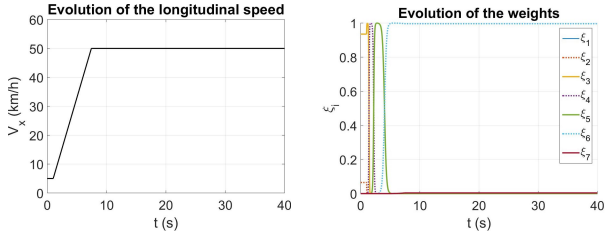

(a) (b)

Fig. 12. Evolution of the longitudinal speed (a) and the weights (b) in function of the time

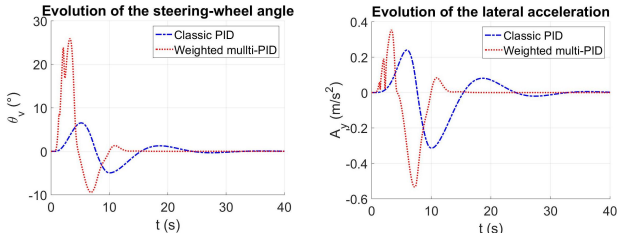

(a) (b)

Fig. 13. Evolution of the steering-wheel (a) and the lateral acceleration (b) in function of the time

The weights evolve (Fig. 12 (b)) accordingly to the speed. During the simulation, 5 weights so 5 PID are used. Even if it does not seem to affect the output, the influence of the weights on others signals like the steering-wheel and the lateral acceleration can be seen on Fig 13 (a) and Fig 13 (b) respectively. Near the speed interval change, the continuity is kept but oscillations can be observed. Because the lateral dynamics of the system is slower with the classic PID, the amplitude of the steering-wheel and the lateral acceleration are smaller. It is important to remark that the steering angle of the wheel (steering column gear ratio $\lambda = 16$) remains small ($B_v(t) < 1.6°$) confirming the assumption considered to obtain the linearized used in the analysis and design of the controllers.

Finally, the weighted multi-PID shows good results for the regulation of the lateral dynamics of the vehicle with variation of the longitudinal speed while a classic PID cannot manage an overtaking if the longitudinal speed is not within its operating area.

VI. CONCLUSIONS

In this paper, an analysis of the vehicle lateral dynamics with the influence of the longitudinal speed has been made. This analysis was used for the design of a weighted PID controller as a function of the longitudinal speed. The weights on the PIDs enable to keep the stability at all speeds whereas a single PID cannot guarantee this stability in all the situations. The calculation of the weights and the intervals depends on the system dynamics. Thus, the method could be used for other systems. Plus, the use of PID make it easier to calculate the controller than using LMI.

Currently, studies are made to prove the stability of the system. Further work could deal with the inclusion of the road adhesion in the design of the controller and the comparison with robust controllers like H_∞ controller or CRONE controller. Other, simulations in the case of intersections or roundabouts could be made and the designed multi-controller could be implanted in a real vehicle.

REFERENCES

[1] R. T. O'Brien, P. A. Iglesias, and T. J. Urban, "Vehicle lateral control for automated highway systems," *IEEE Transactions on Control Systems Technology*, vol. 4, no. 3, pp. 266–273, 1996.

[2] A. Broggi, M. Bertozzi, A. Fascioli, C. G. L. Bianco, and A. Piazzi, "The argo autonomous vehicles vision and control systems," *International Journal of Intelligent Control and Systems*, vol. 3, no. 4, pp. 409–441, 1999.

[3] J. P. Rastelli and M. S. Peñas, "Fuzzy logic steering control of autonomous vehicles inside roundabouts," *Applied Soft Computing*, vol. 35, pp. 662–669, 2015.

[4] J. Pérez, V. Milanés, T. De Pedro, and L. Vlacic, "Autonomous driving manoeuvres in urban road traffic environment: a study on roundabouts," *IFAC Proceedings Volumes*, vol. 44, no. 1, pp. 13795–13800, 2011.

[5] M. A. Sotelo, "Lateral control strategy for autonomous steering of ackerman-like vehicles," *Robotics and Autonomous Systems*, vol. 45, no. 3, pp. 223–233, 2003.

[6] P. Falcone, F. Borrelli, J. Asgari, H. E. Tseng, and D. Hrovat, "Predictive active steering control for autonomous vehicle systems," *IEEE Transactions on control systems technology*, vol. 15, no. 3, pp. 566–580, 2007.

[7] T. Raharijaona, G. Duc, and S. Mammar, "Robust control and/spl mu/-analysis with application to lateral driving assistance," in *Intelligent Transportation Systems, 2003. Proceedings. 2003 IEEE*, vol. 1, pp. 247–252, IEEE, 2003.

[8] P. Hingwe and M. Tomizuka, "Experimental evaluation of a chatter free sliding mode control for lateral control in ahs," in *American Control Conference, 1997. Proceedings of the 1997*, vol. 5, pp. 3365–3369, IEEE, 1997.

[9] W. Chee and M. Tomizuka, "Lane change maneuver of automobiles for the intelligent vehicle and highway system (ivhs)," in *American Control Conference, 1994*, vol. 3, pp. 3586–3587, IEEE, 1994.

[10] J. E. Naranjo, C. Gonzalez, R. Garcia, and T. De Pedro, "Lane-change fuzzy control in autonomous vehicles for the overtaking maneuver," *IEEE Transactions on Intelligent Transportation Systems*, vol. 9, no. 3, pp. 438–450, 2008.

[11] A. L. Kornhauser, "Neural network approaches for lateral control of autonomous highway vehicles," in *Vehicle Navigation and Information Systems Conference, 1991*, vol. 2, pp. 1143–1151, IEEE, 1991.

[12] A. Benine-Neto, S. Mammar, B. Lusetti, and S. Scalzi, "Piecewise affine control for lane departure avoidance," *Vehicle System Dynamics*, vol. 51, no. 8, pp. 1121–1150, 2013.

[13] S. Mammar, N. Minoiu-Enache, S. Glaser, B. Lusetti, and A. Benine-Neto, "Lane keeping automation at tire saturation," in *Proceedings of the IEEE American Control Conference, Baltimore*, pp. 6466–6471, June 2010.

[14] H. Pacejka, *Tire and vehicle dynamics*. Elsevier, 2005.

[15] N. Monot, X. Moreau, A. Benine-Neto, A. Rizzo, and F. Aioun, "Dynamic Stability Control system: the CRONE approach ," *IFAC-PapersOnLine*, vol. 50, no. 1, pp. 13822 – 13827, 2017.

[16] D. Liberzon and A. S. Morse, "Basic problems in stability and design of switched systems," *IEEE Control systems*, vol. 19, no. 5, pp. 59–70, 1999.

[17] V. De Oliveira and A. Karimi, "Robust and gain-scheduled pid controller design for condensing boilers by linear programming," *IFAC Proceedings Volumes*, vol. 45, no. 3, pp. 335–340, 2012.

[18] T. Shamir, "How should an autonomous vehicle overtake a slower moving vehicle: Design and analysis of an optimal trajectory," *IEEE Transactions on Automatic Control*, vol. 49, no. 4, pp. 607–610, 2004.